


PAPER

Magnetic-tunable sound absorber based on micro-perforated magnetorheological elastomer

To cite this article: Xufeng Cao *et al* 2020 *Smart Mater. Struct.* **29** 015024

View the [article online](#) for updates and enhancements.

Magnetic-tunable sound absorber based on micro-perforated magnetorheological elastomer

Xufeng Cao¹, Shouhu Xuan^{1,2,4}, Jun Li³, Zhiyuan Li³, Tao Hu¹, Haiyi Liang^{1,2}, Li Ding¹, Binshang Li³ and Xinglong Gong^{1,2,4} 

¹CAS Key Laboratory of Mechanical Behavior and Design of Materials, Department of Modern Mechanics, CAS Center for Excellence in Complex System Mechanics, University of Science and Technology of China, Hefei 230027, People's Republic of China

²IAT-Chungu Joint Laboratory for Additive Manufacturing, Anhui Chungu 3D printing Institute of Intelligent Equipment and Industrial Technology, Wuhu, Anhui 241200, People's Republic of China

³Anhui Weiwei Rubber Parts Group Co. Ltd, Tongcheng, Anhui 231400, People's Republic of China

E-mail: xuansh@ustc.edu.cn and gongxl@ustc.edu.cn

Received 6 July 2019, revised 29 September 2019

Accepted for publication 14 November 2019

Published 2 December 2019



CrossMark

Abstract

A novel resonance sound absorber, whose resonant frequency characteristic can be varied by turning the external magnetic field, is constructed based on micro-perforated magnetorheological elastomer (MP-MRE). The influence of parameters, such as porosity, thickness, curing agent weight ratio and magnetic field intensity, are investigated to analyze the magneto-acoustic coupling property of MP-MRE sound absorber. By increasing the magnetic flux density, the resonant frequency of resonance sound absorber moves toward high frequency region. It is found the magnetic field-induced deformation of the MP-MRE and its pores affected the resonant frequency. When the magnetic flux density was increased from 0 to 132 mT, the maximum variation of the resonant frequency reached 304 Hz. Finally, originated from this unique magnetic controllability, the MP-MRE sound absorber shows broad potential in the tunable sound absorber at middle and low frequency range.

Supplementary material for this article is available [online](#)

Keywords: magnetorheological elastomer, magnetic properties, micro-perforated, resonant frequency, sound absorber

(Some figures may appear in colour only in the online journal)

1. Introduction

Conventional sound absorbing materials can be divided into resonance sound absorbing structures [1–3] and porous sound absorbing materials [4, 5] according to their sound absorption mechanism [6]. As a kind of resonance sound absorbing structure, the micro-perforated panel (MPP) is composed of the thin panel with a perforation diameter of ≤ 1 mm and the rear cavity of the panel. Since Maa firstly proposed the basic theory and design principles of MPP [7], sound absorbing

structures based on MPP theory have been extensively developed [8–11] in noise control field [12–15]. The MPP has wider sound absorption bandwidth than perforated plate and exhibits better absorption characteristics than sheet resonance absorption materials. Compared with porous and fibrous materials possessing similar absorption characteristics, the MPP with relatively thin thickness can achieve high sound absorption coefficients. Therefore, the MPP is one of the most attractive sound absorbing material and has promising applications in the noise control field.

Usually, the resonant frequency of the conventional MPP sound absorbing structure was mainly tuned by mechanically

⁴ Authors to whom any correspondence should be addressed.

changing the cavity size with screw structure or stepping motor [16]. In comparison to the mechanical tuning method, the electric and magnetic tuning method has real-time controllability and does not require discrete mechanical parts. In recent studies, electric actuation has been introduced in tuning the resonant frequency of sound absorbing structure. Chang *et al* [17] used shunt damping technology to control the sound absorption property of MPP coated with piezoelectric material and electrical circuits. Duan *et al* [18] developed a flexible MPP absorber which was composed of a perforated aluminum-electrode Polyvinylidene fluoride piezoelectric film. Tao *et al* [19] proposed a finite MPP backed by a shunted loudspeaker. The result showed the resonance characteristics could be adjusted by changing the electrical parameters in the shunted circuit. Lu *et al* [20] presented an electrically tunable acoustic absorber based on a micro-perforated dielectric elastomer actuator. The active shifting of the acoustic absorption spectrum could be achieved by voltage activation that reduced the membrane tension and holes size.

Besides the electrically tunable acoustic absorber, the magnetic tuning method is also gradually developed for the resonance sound absorbing structure, due to the simple structure, remote contactless control and quick response capability [21–25]. In this area, the magnetorheological elastomer (MRE) is the mostly used material. MRE is a kind of smart materials with enticing prospect in magnetic manipulation [26–28]. It is usually consisting of three components: soft elastomer matrix, additives and magnetic particles [29], which has remote contactless magnetic actuation and quick response capability [30–32]. By decreasing the thickness, the MRE shows good magnetic-induced deformation performance [33–36]. Schmauch *et al* [37] realized the directional actuation of elastomer films with chains of magnetic nanoparticles aligned. Due to this magnetic phenomenon, Mahendran *et al* [38] found that Ni-Mn-Ga/polymer magnetic composites showed a good acoustic attenuation. Moreover, Chen *et al* [22] designed a magneto-acoustic metamaterial based on magnetorheological elastomer, and they observed that the resonant frequency was tunable by the external gradient magnetic field. Therefore, due to the excellent magnetic-induced deformability, the thin MRE is of enticing prospect for wide application in acoustic absorber.

Obviously, the acoustic properties of MRE have attracted the interests of many researchers. Chiu *et al* [21] found that the magnetic field showed high influence on the transmission loss spectrum of a drum-like silencer consisting of cavities covered by ferromagnetic membranes. Nguyen *et al* [25] developed an analytical vibro-acoustic-electromagnetic coupling model to study magneto-based acoustic metamaterials. Hasheminejad *et al* [39] developed a two-dimensional analysis damping model to investigate the acoustic insulation characteristics of the sandwich plate based on magnetorheological elastomeric core. Moreover, the acoustic properties of other MR based structures are also been investigated [24, 40–42]. These works took full advantage of the controllable stiffness of magnetic materials. Although some researches have been conducted on the acoustic insulation characteristics

of MRE with the solid structure, few works have been focused on the sound absorption property of micro-perforated structure MRE. Considering the good sound absorption characteristics of the micro-perforated structure and excellent magnetic-induced deformation properties of MRE, the investigation of a magnetic-tunable resonance sound absorber based on the micro-perforated structure MRE is pressing needed. Compared with the traditional MPP sound absorber, the novel absorber has the advantages of fast response capability, real-time controllability and efficient, offering a new magnetic tuning method in the sound absorption control of MPP absorber.

This work reported a micro-perforated magnetorheological elastomer (MP-MRE) sound absorber with good flexibility, stability and magnetic sensitivity. The influence of porosity, curing agent ratio, thickness and magnetic field intensity on magnetic-induced deformation and sound absorption property of MP-MRE sound absorber were investigated. Meanwhile, the magnetic-induced deformation was found to be very important for understanding the mechanic-magnetic-acoustic coupling behavior of MP-MRE sound absorber. Because of the micro-perforated structure and magnetic actuation properties, MP-MREs sound absorber showed good sound absorption and tunable resonant frequency properties. Finally, a novel magnetic-tunable sound absorber based on MP-MRE was developed and it further proved the reliability of MP-MRE sound absorber.

2. Experiment section

2.1. Materials

The polydimethylsiloxane (PDMS) precursor and curing agent used here were all purchased from Dow Corning GmbH, USA. The carbonyl iron particles (CIPs) with an average diameter of 7 μm , used as magnetic filler, were provided by BASF in Germany.

2.2. Fabrication

The fabrication processes of MP-MREs sound absorber were illustrated in figure 1. Firstly, PDMS precursor with different curing agent weight ratio (1:10, 1:15 and 1:20) and CIPs were mixed for 10 min in a beaker, and subsequently sonicated for 10 min to make the CIPs to be homogeneously dispersed. Here, curing agent weight ratio was the ratio of curing agent to PDMS precursor. The weight fraction of CIPs was kept at 50 wt% for all samples. Then, the beaker was transferred into a vacuum container and degassed for 20 min. After that, the sample was molded and vulcanized in the molds with a diameter of 116 mm at 100 °C under 20 MPa for 10 min. Next, the resulting MREs with a thickness of 0.5, 0.75, 1 and 1.25 mm were transferred into a laser processing platform. After laser ablation, the MP-MRE was obtained, and the diameter of the hole was about 800 μm . Finally, the MP-MREs were fixed to the holder on the surface of the rigid wall

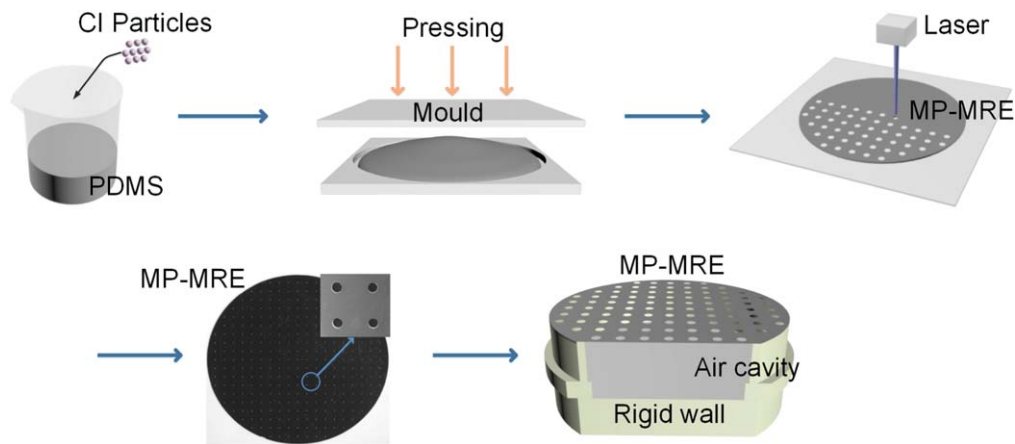


Figure 1. Fabrication processes of MP-MREs sound absorber.

to form an air cavity, then the whole structure was combined into the MP-MRE sound absorber.

2.3. Characterization

The morphology of MP-MREs was characterized by scanning electron microscopy (SEM, GeminiSEM 500, ZEISS) under 16 kV. The storage modulus of the MP-MREs was measured by using a rheometer (Physica MCR 301, Anton Paar Co., Austria). MP-MREs with a diameter of 2 cm and a thickness of 1 mm were tested under the normal force of 1 N. The shear frequency was 5 Hz and the shear strain was 0.1%. The uniaxial tension test of the samples was carried out by a universal test machine (MTS criterion 43, MTS System Co., America). The samples were cut into a rectangle shape and the tensile rate was set as 2 mm min^{-1} .

The digital image correlation (DIC) method was applied to measure the magnetic-induced deformation of the MP-MREs sound absorber. A kind of white paint was sprayed onto the surface of MP-MREs to obtain the speckle pattern. Stereo cameras were used to record and capture images of the speckle pattern for calculating the deformation. The MP-MREs were fixed on a 3D print holder with a height of 12 mm and an outer diameter of 100 mm. Then the assemblage was fixed on the top surface of the electromagnet to form a cavity. A programmable direct-current (DC) power device was used to produce the step current. When the output current was set at 1.5, 3 and 4.5 A, the measured magnetic flux density at the center of the initial position of the sample reached 56, 98 and 132 mT, respectively. The simulated magnetic field distribution was shown in figure S1 is available online at stacks.iop.org/SMS/29/015024/mmedia. All of the correlation computation processes were conducted on a commercial DIC analyzer (PMLAB DIC-3D, Nanjing PMLAS Sensor Tech. Co., Ltd).

The acoustic absorption property of MP-MREs sound absorber was measured by an impedance tube device (Bswa Technology Co., China) according to ISO 10534-2, and the sound absorption coefficient was analyzed by the transfer function method. The frequency range for this study was between 250 and 1600 Hz. The impedance tube was

composed of a sound source, microphones and a sample holder. The MP-MREs were placed in the sample holder to ensure that the distance between samples and electromagnet surface was 12 mm. The same magnetic field generation method had been described as before. The diameter of MP-MRE samples was 100 mm and thickness was varied from 0.5 to 0.75, 1 and 1.25 mm. The holes were distributed in a square array, and the ratio of the micro-perforated area to the total area was defined as the porosity. The porosity of the MP-MREs was 0.5%, 1.0%, 1.5% and 2.0%, respectively.

3. Results and discussions

3.1. Characterization of MP-MREs

As shown in figures 2(a)–(d), the holes were distributed in a square array with different spacing, and the porosity of the samples was 0.5%, 1.0%, 1.5% and 2.0%, respectively. Figure 2(e) showed the SEM image of a single hole. Obviously, the diameter of the hole was about $800 \mu\text{m}$, and the boundary was very smooth and continuous. Besides, the surface micrograph of MP-MRE demonstrated that the CIPs were uniformly distributed in the PDMS matrix without significant agglomeration phenomenon (figure 2(f)).

The storage modulus of the MP-MREs was measured by using a rheometer. Keeping curing agent weight ratio of 1:15, the storage modulus of MP-MREs with different porosity was tested (figure 3(a)). With the increasing of porosity, the initial shear storage modulus decreased firstly and then increased gradually. The reason was that the prestress would increase significantly with the porosity due to the constant normal force, which could affect the initial storage modulus. With increasing of magnetic field, the storage modulus gradually increased and reached a steady state after the magnetic field was larger than 600 mT. Moreover, keeping the porosity constant, the storage modulus of the MP-MREs with different curing agent weight ratio was investigated (figure 3(b)). Clearly, with increasing of curing agent weight ratio, the initial storage modulus increased, which demonstrated the weakening of deformation capacity. Furthermore, it could be

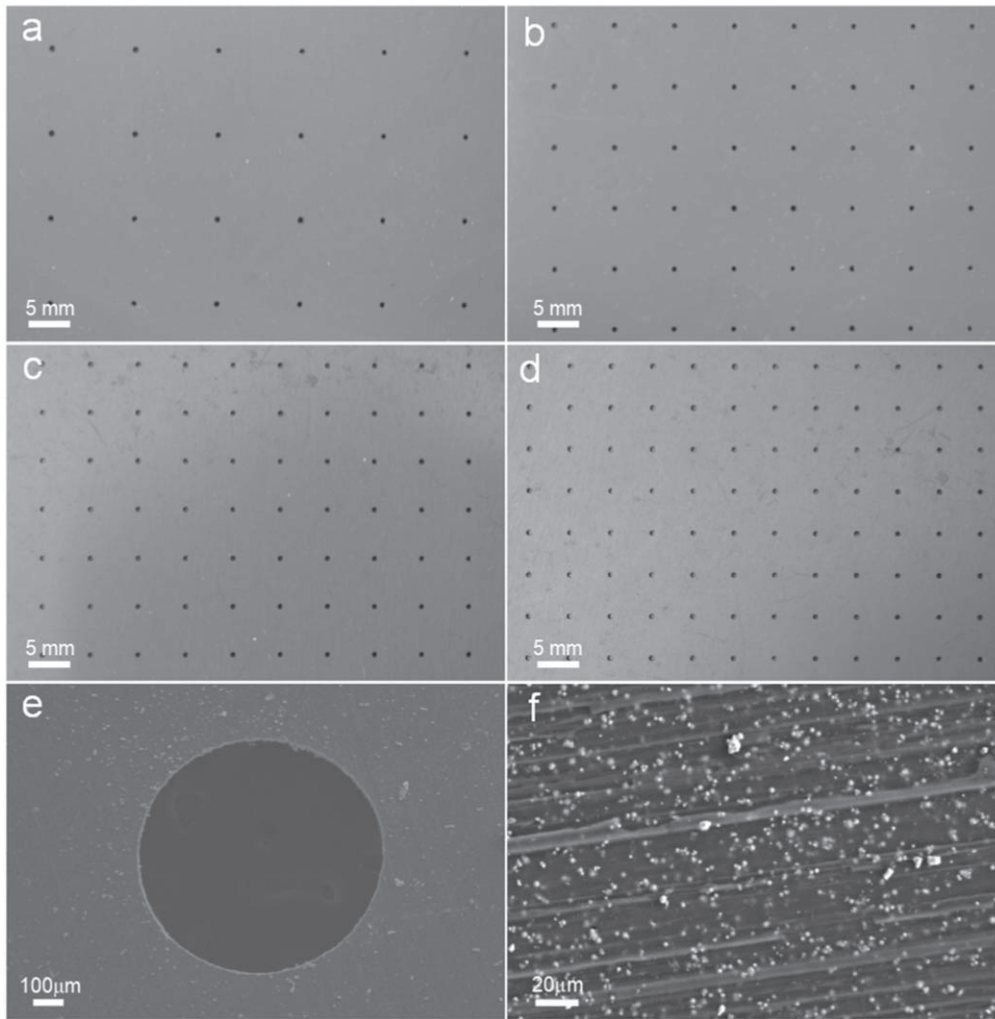


Figure 2. (a)–(d) Optical images of porosity of MP-MREs; and SEM images of (e) a single hole; (f) MP-MRE.

seen the storage modulus increased with the increasing of magnetic field, which enhanced the magnetic-induced-stiffness.

The mechanical properties of the MP-MREs under uniaxial tension were studied. Keeping curing agent weight ratio of 1:15, the tensile properties of MP-MREs with different porosity were tested at 2 mm min^{-1} (figure 3(c)). Clearly, under the low tensile strain, the stress–strain curve of all samples was basically coincident and showed excellent elasticity. Here, this phenomenon must be responded for that the number of submillimeter holes increased slightly due to the lower porosity. Moreover, keeping porosity of 0.5%, the effect of curing agent weight ratio on tensile properties was investigated (figure 3(d)). If the strain was smaller than 20%, the tensile stress increased linearly with tensile strain, which showed the ideal elastic deformation of samples. With increasing of curing agent weight ratio from 1:20 to 1:10, although the fracture strain decreased from 0.88 to 0.48, the fracture stress increased from 0.37 to 1.62 MPa. The interaction of PDMS molecular chains increased with the curing agent weight ratio, the tensile strength and Young's modulus increased significantly, so the deformation capacity reduced. For all samples, when the strain exceeded 20%, the stress–

strain curve gradually began to show nonlinear behavior. In summary, the mechanical properties of MP-MREs demonstrated good elasticity, flexibility, and stability under small deformation.

3.2. Magnetic-induced deformation of the MP-MREs sound absorber

As a kind of soft magnetic material, the CIPs could be easily magnetized under the external magnetic field. According to the classical magnetic dipole model, the relations between the magnetic dipole moment \vec{m} and the magnetic flux density \vec{B} could be obtained by [43]

$$3\hat{n}\hat{n} \cdot \vec{m} - \vec{m} = \frac{4\pi r^3}{\mu_0} \vec{B}, \quad r > 0, \quad (1)$$

where μ_0 was the permeability of vacuum, r was the radius of the magnetic dipole and \hat{n} was the unit vector of \hat{r} . When the magnetic dipole was in gradient magnetic field, the mutual magnetic attractive force could be obtained by [43]

$$\vec{F} = \nabla(\vec{m} \cdot \vec{B}). \quad (2)$$

Hence, the elastomer with the magnetic particle fillers could

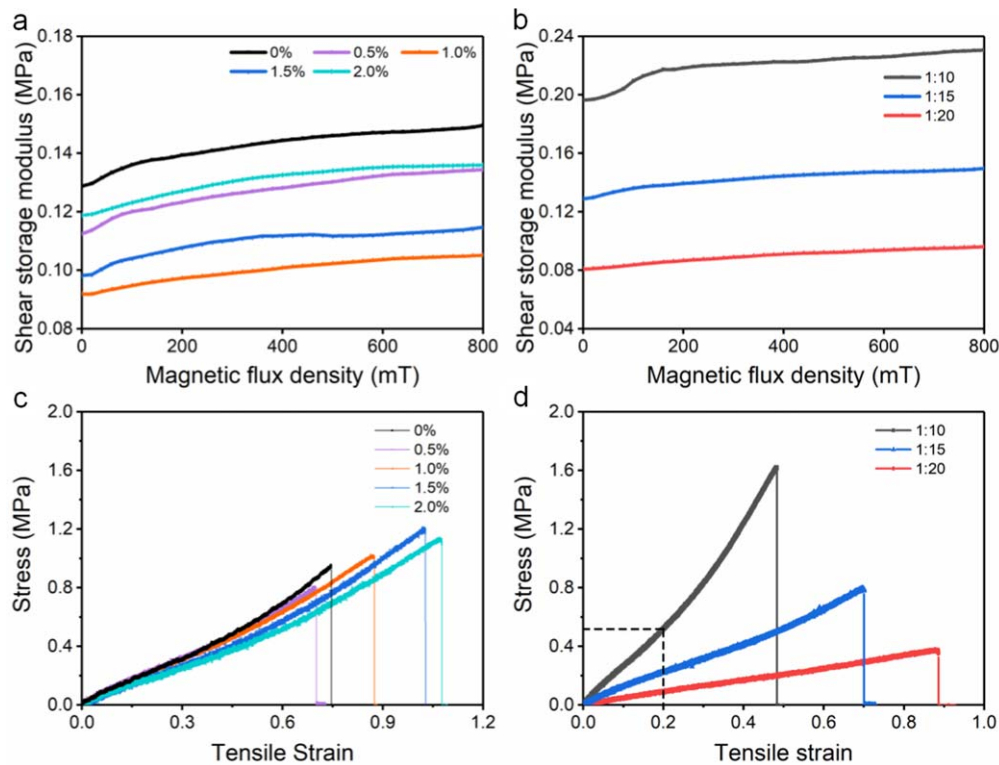


Figure 3. The storage modulus versus the magnetic flux density of (a) the MP-MREs with different porosity; (b) different curing agent weight ratio; and the stress–strain curve of (c) the MP-MREs with different porosity; (d) different curing agent weight ratio.

be deformed due to the interaction between magnetic dipole and the external gradient magnetic field. Therefore, the MP-MREs showed a typical magnetic-induced deformation. The DIC method was applied to measure the magnetic-induced deformation of the MP-MREs (figure 4(a)). A programmable DC power device provided step currents (1.5, 3 and 4.5 A) which generated different magnetic fields (56, 98 and 132 mT) at the center of the initial position of the sample. For convenience, the current data during experiments were used to represent the corresponding magnetic fields in the following discussion.

In the initial state, the MP-MREs was vertically positioned and fixed on a 3D print holder. Then, by applying different current to the electromagnet, the longitudinal deformation increased firstly and then became stable. Here, a symmetrical deformation was found under the external gradient magnetic field. For the sample with porosity of 0.5%, thickness of 1 mm and curing agent weight ratio of 1:10, the out-plane displacements of the sample under different magnetic field were studied (figures 4(b)–(d)). The XY axial indicated the position of the sample during the test. The maximum displacement varied from 2.90 to 6.31 mm under the currents from 1.5 to 4.5 A. Obviously, the maximum out-plane displacement occurred nearly at the center of samples and increased significantly with magnetic field (figure 4(e)).

To further characterize the detailed deformation, the displacement curves of X–Z plane at the center of the MP-MRE under different magnetic field were extracted to analyze the deformation (figure 4(f)). The results showed the out-plane deformation was symmetrical and the maximum

occurred at the center of samples. As expected, the trend of deformation under different current was the same. Figure 4(g) showed the schematic diagram of the magnetic-induced deformation behavior. According to the formula (2), with the increasing of magnetic flux density, the attraction force between magnetic field and CIPs increased, the PDMS further deformed. In this case, the elastic force balanced the attraction force.

For the MP-MREs sound absorber with the different porosity, thickness and curing agent weight ratio, the maximum displacement of all samples significantly increased with the currents from 1.5 to 4.5 A (figures 4(h)–(j)). As shown in figure 4(h), for a constant thickness of 1 mm and curing agent weight ratio of 1:10, with the increasing of porosity, the out-plane displacement was basically coincident under the same current condition. Figure 4(i) showed the effect of the thickness on out-plane deformation. When thickness changed from 0.5 to 1.25 mm, the maximum displacement increased firstly and kept constant under the same magnetic field. With increasing of curing agent weight ratio, Young's modulus significant increased, which significantly decreased the maximum displacement from 11.57 to 6.31 mm under the current of 4.5 A (figure 4(j)).

In addition, the deformation characteristics of holes under applying the external magnetic field were studied. Figure 5(a) showed the digital photograph of the test system of MP-MREs sound absorber. Since the deformation of MP-MREs was centro-symmetrical, a row of holes on a radius were selected as observation objects to show the deformation characteristics. Due to the good magnetic-induced

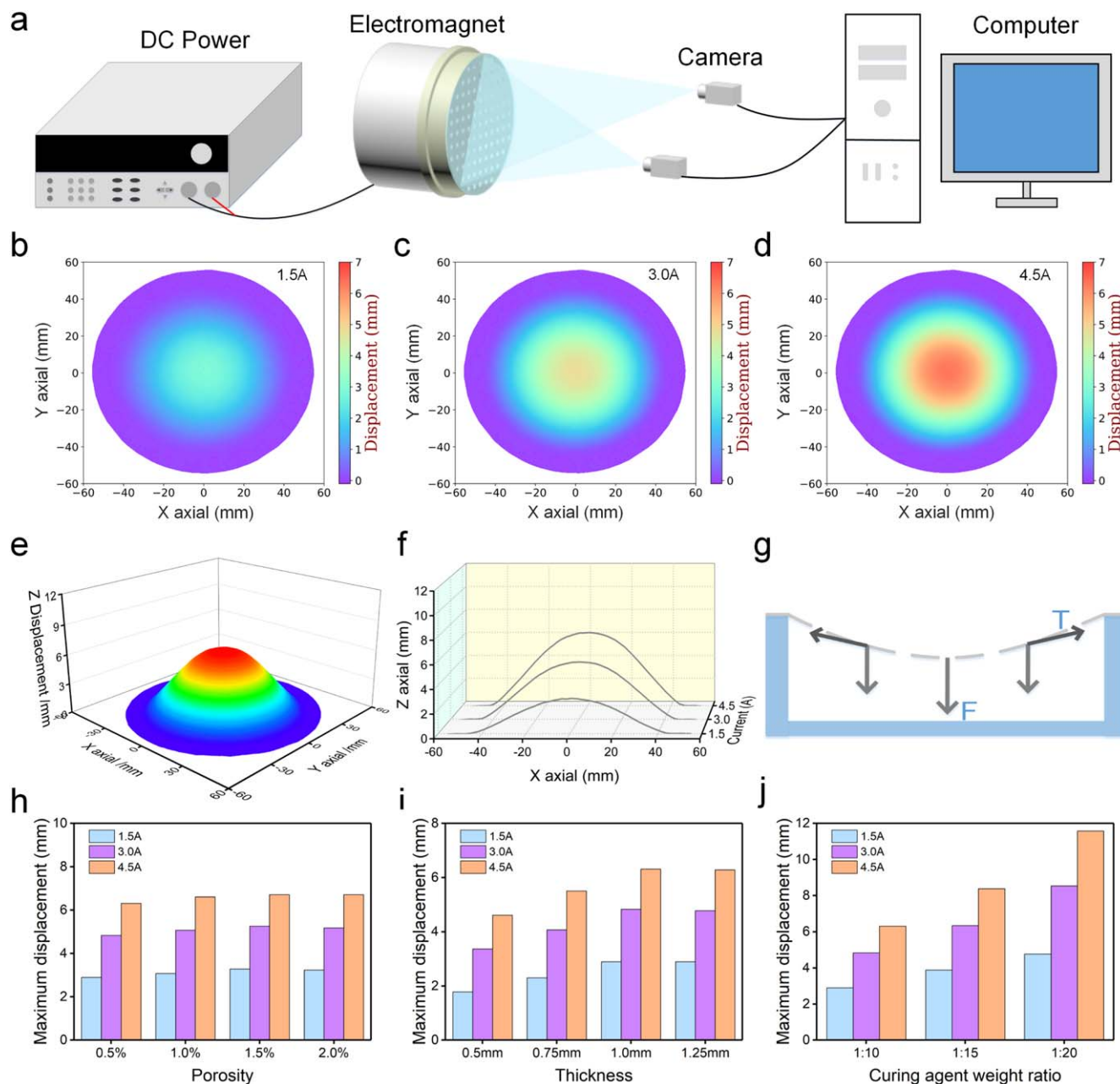


Figure 4. (a) Schematic illustration of the digital image correlation (DIC) method; (b)–(d) The out-plane displacements of the MP-MRE with different current from 1.5 to 4.5 A; (e) Deformation diagram of MP-MRE; (f) Displacement curves of X–Z plane passed through the center of the circle under different magnetic field; (g) Schematic diagram of the magnetic-induced deformation behavior; (h)–(j) The maximum displacement of MP-MREs sound absorber with different porosity, thickness and curing agent weight ratio.

deformation properties, the sample with porosity of 0.5%, thickness of 1 mm and curing agent weight ratio of 1:15 was selected for further discussion.

As shown in figure 5(b), the red dotted circle was the microporous boundary after a 4.5 A current was applied in the electromagnet. Obviously, the microporous array was changed by translation. Moreover, the shape and size of microporous array were also changed. Since the microscope was perpendicular to the initial position of the sample, once the MP-MRE was deformed, the circular shape observed in the microscopic field was actually elliptical shape (figure 5(c)). The reason was that the radial deformation was greater than

the circumferential deformation during the deformation process. Therefore, the area of the ellipse could be calculated by the circle size and the tilt rate of the sample. Here, the relative area variation of the holes was defined as $\Delta S/S_0 = (S - S_0)/S_0$ in which S_0 was the initial area, S was the area under the magnetic field and ΔS was area variation. The relative area variation of holes on radius was shown in figure 5(d). Interestingly, the minimum area variation occurred at the circumference near $D/2$, and the area variation of the hole numbered VI on the fixed boundary was basically unchanged. After tuning the current to 0 A, the MP-MREs deformation recovered and the shape of holes also changed

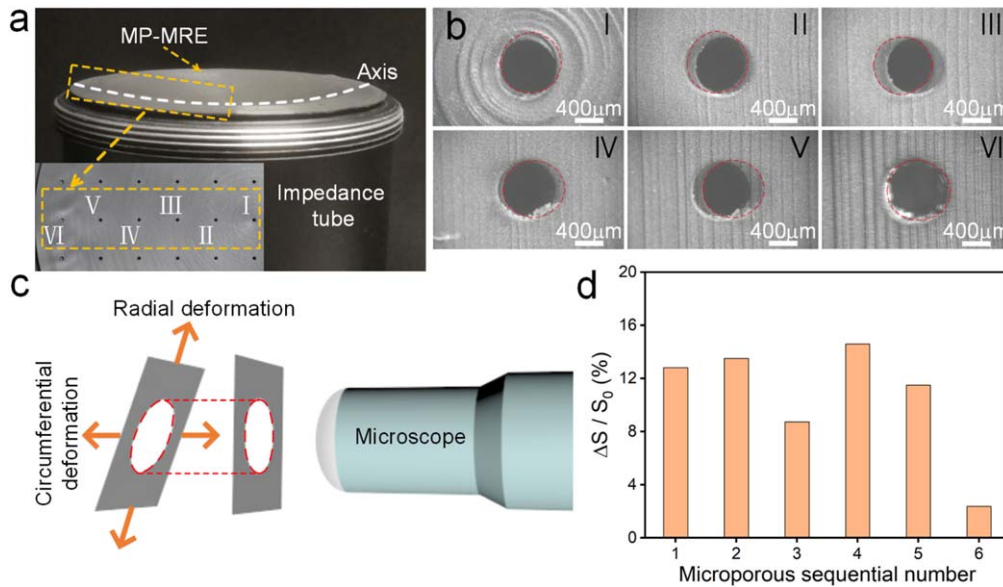


Figure 5. (a) The test system of MP-MREs sound absorber; (b) Optical images of a row of holes on a radius; (c) Schematic illustration of the difference of the actual elliptical and the circular shape seen in the field of view; (d) The relative area variation of holes.

from ellipse to circle. In summary, due to the small out-plane displacement, when the current was turned off, the MP-MREs sound absorber recovered to the initial state, exhibited excellent stability and reliability.

3.3. Acoustic performance of the MP-MREs sound absorber

The sound absorption properties of MP-MREs sound absorber were measured by an impedance tube device (figure 6(a)). The air cavity depth was 12 mm in impedance tube. Here, because the sample holder covered some holes while the test area remained unchanged, the porosity of MP-MREs sound absorber was calculated to be decreased from 0.5%, 1.0%, 1.5% and 2.0% to 0.39%, 0.74%, 1.11% and 1.48%, respectively. Figure 6(b) showed the sound absorption property of the MP-MRE and pure MRE. Obviously, MP-MRE sound absorber had wider frequency range of absorption and higher sound absorption coefficient than the MRE. Due to the magnetic-induced deformation of the MP-MREs sound absorber, its resonant frequency was changeable under applying the magnetic field. For the sample with porosity of 0.39%, thickness of 1 mm and curing agent weight ratio of 1:10, the sound absorption properties of the sample under different magnetic field were shown in figure 6(c). Here the variation of the resonant frequency was defined as $\Delta f = f_i - f_0$ in which f_0 was initial resonant frequency under the 0 A, f_i was the corresponding resonant frequency under the magnetic field.

Figures 6(d)–(f) showed the sound absorption property of the MP-MREs sound absorber under various testing parameters. Clearly, the MP-MREs sound absorber significantly reduced the acoustic noise nearly the resonant frequency. Since the micro-perforated structure, when the acoustic wave flowed into the interior of the submillimeter hole, it would lead to the vibration of air. Due to the frictional and viscous resistance, the acoustic energy would be transformed into

thermal energy [14]. When the frequency of the incident acoustic wave was close to the resonant frequency, the vibration velocity and amplitude of the air column and the sound energy dissipation significantly increased, thus the sound absorption coefficient reached the maximum value. Conversely, when the frequency of the sound wave was far from the resonant frequency, the vibration of the air in the system was reduced, so the sound absorption coefficient decreased. The sound absorption coefficient varied with the frequency of applied acoustic wave, and the maximum absorption coefficient appeared at the resonant frequency of the system.

Furthermore, the porosity of the MP-MREs sound absorber played an important role in the resonant frequency. For a constant thickness of 1 mm and curing agent weight ratio of 1:10, with the increasing of the porosity, the resonant frequency of MP-MREs sound absorber moved toward high frequency region and the width of the frequency band were increased. The sound absorption peaks were 0.908, 0.992, 0.993 and 0.969, which occurred at 704 Hz, 952 Hz, 1150 Hz and 1328 Hz, respectively. In addition, with increasing of the thickness, the resonant frequency and maximum absorption coefficient were significantly decreased. Keeping the porosity (0.39%) and curing agent weight ratio (1:10) as constant, they changed from 0.992 at 864 Hz to 0.878 at 634 Hz due to the increased acoustic resistance with the thickness [44]. At last, the influence of the curing agent weight ratio on the sound absorption property of MP-MREs absorber was also investigated. The results showed the resonant frequency of MP-MREs absorber was barely affected by the curing agent weight. For a constant porosity of 0.39% and thickness of 1 mm, the maximum absorption coefficient of samples was about 0.972 at 792 Hz.

Additionally, the resonant frequency of all MP-MREs sound absorber was significantly affected by magnetic field. With the increasing of the current from 0 to 4.5 A, the

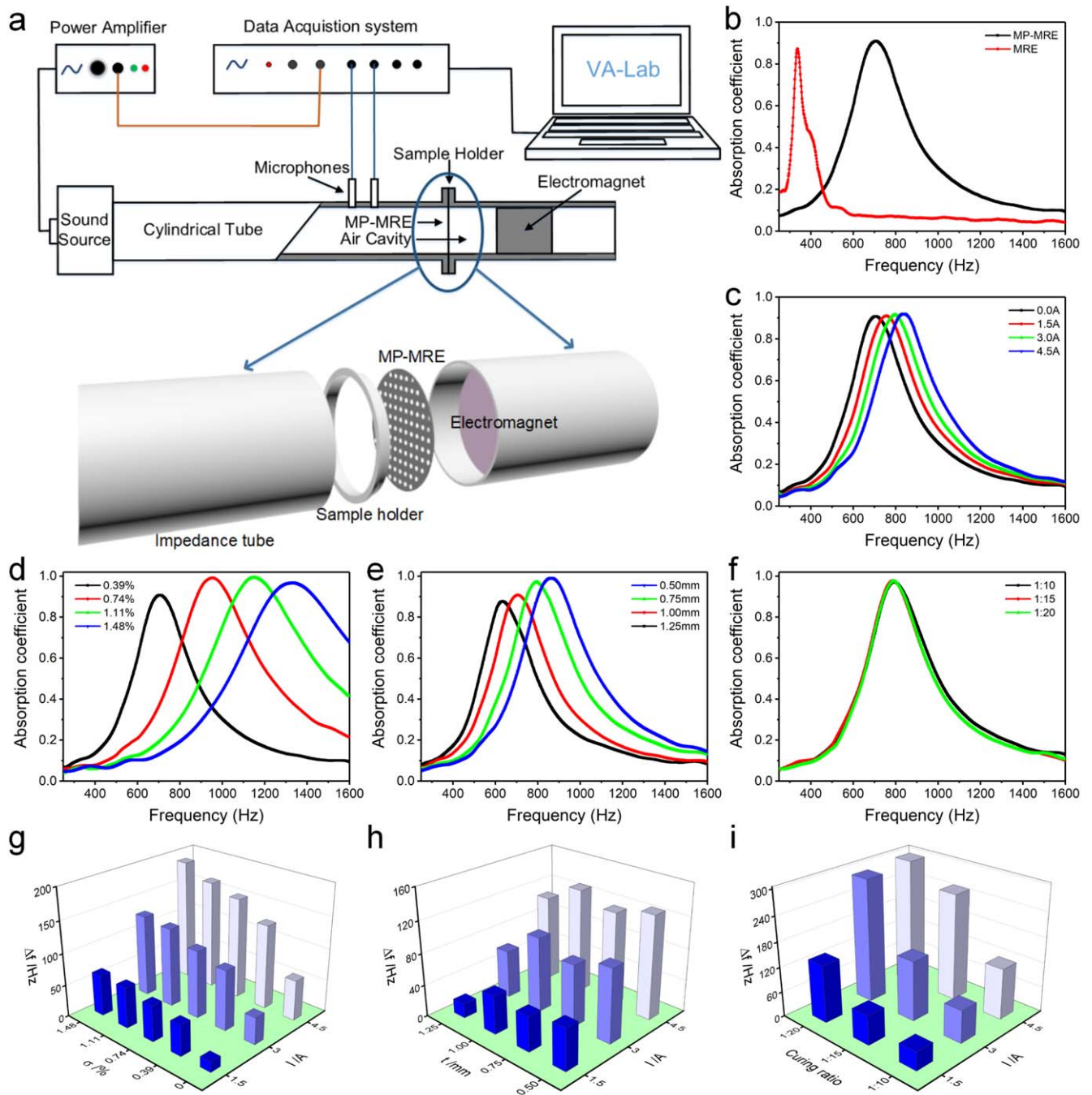


Figure 6. (a) Schematic illustration of the measurement system based on impedance tube; (b) The measured sound absorption property of the MP-MRE and pure MRE; (c) The measured sound absorption property of the MP-MRE sound absorber under the different current; (d)–(f) The measured sound absorption property of the MP-MREs sound absorber with different porosity, thickness and curing agent weight ratio; (g)–(i) The variation of resonant frequency of MP-MREs sound absorber with different porosity, thickness and curing agent weight ratio under the different magnetic field.

resonant frequency gradually moved toward high frequency region, thus Δf was increased from 18 to 304 Hz (figures 6(g)–(i)). A mechanism was proposed to investigate the mechanic-magnetic-acoustic coupling properties of the MP-MREs sound absorber (figure 7(a)). The magnetic interaction force between the MP-MREs and electromagnet was increased with the current, then the MP-MREs was forced to deform. In this case, the air cavity volume was decreased. Because the effect of air cavity on the sound absorption

property was similar to the thickness, the resonant frequency moved toward high frequency region with the decreasing of the cavity. Besides, the shape and area of the holes were also slightly changed during the deformation process. However, the incident sound wave was perpendicular to the vertical plane, and the projection of the hole on the vertical plane was still circular whose area variation was small. Thus, the effect of the shape change of the holes on the variation of the resonance frequency could be negligible. The variation

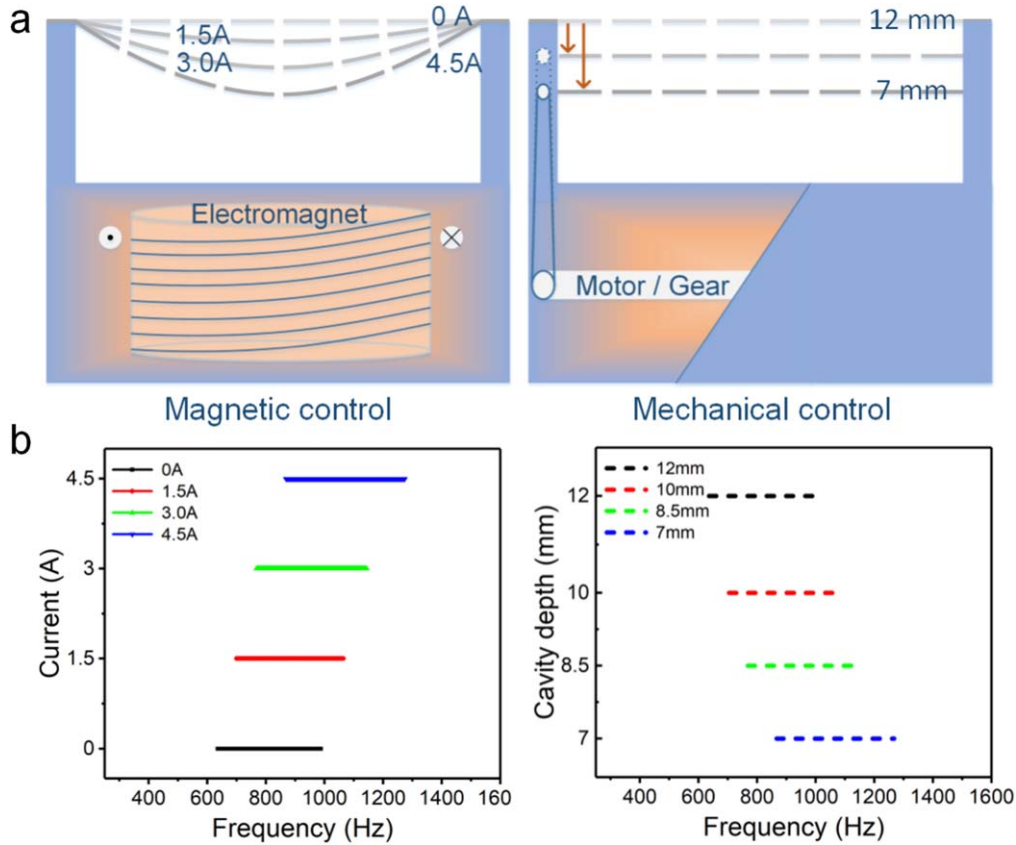


Figure 7. (a) Schematic of magnetic control method and conventional mechanical control method about how to change the resonant frequency; (b) The sound absorption bandwidth with the different magnetic field and cavity depth.

tendency of Δf with the current was similar with the result of the magnetic-induced deformation (figures 4(h)–(j)). Moreover, under the same current, Δf was slightly increased with porosity and significantly increased with the decrease of curing agent weight ratio (figures 6(g), (i)). That was because the elastic modulus slightly decreased with the increase of porosity, and the cross-link density of PDMS matrix gradually increased with curing agent content. As a result, it can be concluded that the MP-MREs sound absorber had a tunable sound absorption property by manipulating the magnetic field.

Compared with traditional MPP sound absorber, the MP-MREs sound absorber provided a new method to change the resonant frequency of sound absorber. Figure 7(a) showed the schematic of different control methods to change the resonant frequency. According to Maa's theory, when the sound absorption coefficient was half the maximum, the corresponding frequency f_1 and f_2 were the half absorption frequencies. The frequency range $f_r = f_2 - f_1$ was called the frequency bandwidth of absorption [7]. As shown in figure 7(b), the length values of the solid line corresponded to the bandwidth under the varied magnetic field. In order to obtain the same sound absorption bandwidth, the corresponding experiment results were conducted with the different cavity depth by changing the cavity depth from 12 to 7 mm. Therefore, the MP-MREs sound absorber could be a tunable sound absorber to change the resonant frequency conveniently by applying different magnetic field.

In practical applications, the initial resonant frequency of the MP-MREs sound absorber should be qualitatively designed. Due to the same submillimeter hole structure, the classic formula of MPP absorber could be used to simulate the sound absorption property of MP-MREs absorber without external gradient magnetic field. According to Maa's theory, the acoustic impedance could be expressed as [44]

$$Z = \frac{32\eta t}{\sigma \rho_0 c d^2} \left[\left(1 + \frac{k^2}{32} \right)^{1/2} + \frac{\sqrt{2}}{32} k \frac{d}{t} \right] + i \frac{\omega t}{\sigma c} \left[1 + \left(9 + \frac{k^2}{2} \right)^{-1/2} + 0.85 \frac{d}{t} \right], \quad (3)$$

where

$$k = d \sqrt{\omega \rho_0 / 4\eta}$$

here, k was the perforation constant, d was the diameter of the submillimeter hole, ω was the angular frequency, ρ_0 was the density of air, η was the coefficient of viscosity, t was the panel thickness, σ was the porosity and c was the velocity of sound. When the MPP and the air cavity behind it were combined into an MPP absorber, the sound absorption coefficient could be expressed as [44]

$$\alpha = \frac{4r}{(1+r)^2 + (\omega m - \cot(\omega D/c_0))^2}, \quad (4)$$

where, r and ωm were the real and imaginary parts of the

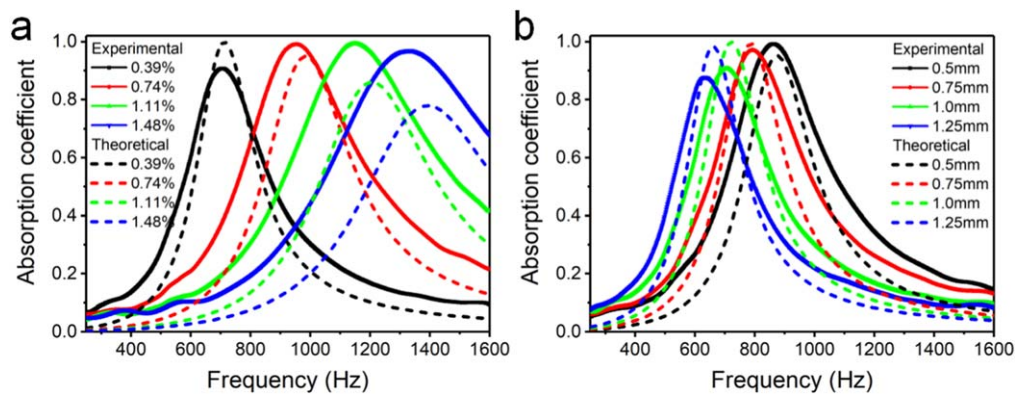


Figure 8. Experimental result of MP-MREs sound absorber with solid line and the theoretical result with dotted line (a) with different porosity; (b) with different thickness.

acoustic impedance Z , which could be calculated by the equation (3). Thus, the theoretical absorption property of MP-MREs sound absorber was calculated by equation (4) with different porosity and thickness.

Figure 8 showed the theoretical result with dotted line and experimental result with solid line. Obviously, the experiment value was close to the theoretical resonant frequency and the maximum error was 4.6%. However, the maximum absorption coefficient had relatively large difference and the maximum deviation was 24.4%. According to the classic Maa's theory, the panel was assumed to be rigid and then the panel vibration could be ignored, and this case led to the deviation between theoretical and experimental data. However, the MP-MREs sound absorber which was based on larger width-thickness ratio and low PDMS matrix modulus could be regarded as a flexible panel, which led to the decrease of the resonant frequency. Therefore, the classic Maa's theory could be used for qualitatively describing and estimating the sound absorption properties of MP-MREs sound absorber without magnetic field. It demonstrated that the initial resonant frequency of MP-MRE sound absorber could be flexibly designed by theory within a specified range of error.

4. Conclusion

In summary, a novel tunable sound absorber with simple structure, wide frequency range of absorption, and tunable resonant frequency was developed based on the MP-MREs. The MP-MREs were demonstrated to have good stretchability, flexibility and stability under tensile loading. By applying magnetic field, the magnetic-induced deformation of MP-MREs sound absorber increased significantly. Besides, the effect of porosity, thickness and curing agent weight ratio was investigated as well. Furthermore, with the increasing of current, the resonant frequency of MP-MREs sound absorber moved toward high frequency region, and variation of resonant frequency was significantly increased, which indicated MP-MREs sound absorber could serve as a tunable sound absorber. Finally, the good magnetic-mechanical-acoustic coupling performance made MP-MREs sound absorber as a

prospective sound absorbing structure and provide a new control method for resonance sound absorber devices.

Acknowledgments

Financial supports from the National Natural Science Foundation of China (Grant Nos. 11822209, 11572310, 11572309, 11972343) and the Strategic Priority Research Program of the Chinese Academy of Sciences (Grant No. XDB22040502) are gratefully acknowledged. This work was also supported by the Collaborative Innovation Center of Suzhou Nano Science and partially carried out at the USTC Center for Micro and Nanoscale Research and Fabrication.

ORCID iDs

Xinglong Gong  <https://orcid.org/0000-0001-6997-9526>

References

- [1] Starkey T A, Smith J D, Hibbins A P, Sambles J R and Rance H J 2017 Thin structured rigid body for acoustic absorption *Appl. Phys. Lett.* **110** 041902
- [2] Kim B-S and Park J 2018 Double resonant porous structure backed by air cavity for low frequency sound absorption improvement *Compos. Struct.* **183** 545–9
- [3] Abbad A, Rabenorosoa K, Ouisse M and Atalla N 2018 Adaptive Helmholtz resonator based on electroactive polymers: modeling, characterization, and control *Smart Mater. Struct.* **27** 105029
- [4] Park J, Yang S H, Minn K S, Yu C B, Pak S Y, Song Y S and Youn J R 2018 Design and numerical analysis of syntactic hybrid foam for superior sound absorption *Mater. Des.* **142** 212–20
- [5] Xue B, Li R, Deng J G and Zhang J H 2016 Sound absorption properties of microporous poly(vinyl formal) foams prepared by a two-step acetalization method *Ind. Eng. Chem. Res.* **55** 3982–9
- [6] Yang M and Sheng P 2017 Sound absorption structures: from porous media to acoustic metamaterials *Annu. Rev. Mater. Res.* **47** 83–114

- [7] Maa D Y 1975 Theory and design of microperforated panel sound-absorbing constructions *Sci. Sin.* **18** 55–71
- [8] Kim H-S, Ma P-S, Kim S-R, Lee S-H and Seo Y-H 2018 A model for the sound absorption coefficient of multi-layered elastic micro-perforated plates *J. Sound Vib.* **430** 75–92
- [9] Mosa A I, Putra A, Ramlan R, Prasetyo I and Esraa A-A 2019 Theoretical model of absorption coefficient of an inhomogeneous MPP absorber with multi-cavity depths *Appl. Acoust.* **146** 409–19
- [10] Ren S W, Van Belle L, Claeys C, Xin F X, Lu T J, Deckers E and Desmet W 2019 Improvement of the sound absorption of flexible micro-perforated panels by local resonances *Mech. Syst. Signal. Process.* **117** 138–56
- [11] Meng H, Galland M A, Ichchou M, Bareille O, Xin F X and Lu T J 2017 Small perforations in corrugated sandwich panel significantly enhance low frequency sound absorption and transmission loss *Compos. Struct.* **182** 1–11
- [12] Park S-H 2013 A design method of micro-perforated panel absorber at high sound pressure environment in launcher fairings *J. Sound Vib.* **332** 521–35
- [13] Yu X, Lau S-K, Cheng L and Cui F S 2017 A numerical investigation on the sound insulation of ventilation windows *Appl. Acoust.* **117** 113–21
- [14] Wu F, Xiao Y, Yu D L, Zhao H G, Wang Y and Wen J H 2019 Low-frequency sound absorption of hybrid absorber based on micro-perforated panel and coiled-up channels *Appl. Phys. Lett.* **114** 151901
- [15] Anoshkin A N, Zuiko V Y, Tashkinov M A and Silberschmidt V V 2015 Repair of damage in aircraft composite sound-absorbing panels *Compos. Struct.* **120** 153–66
- [16] Konishi S, Yoda M, Sugiyama S and Akishita S 2000 Tunable acoustic absorber using a micro acoustic hole array *Electr. Commun. Japan* **83** 1–6
- [17] Chang D Q, Liu B L and Li X D 2010 An electromechanical low frequency panel sound absorber *J. Acoust. Soc. Am.* **128** 639–45
- [18] Duan X H, Wang H Q, Li Z B, Zhu L K, Chen R, Kong D Y and Zhao Z 2015 Sound absorption of a flexible micro-perforated panel absorber based on PVDF piezoelectric film *Appl. Acoust.* **88** 84–9
- [19] Tao J C, Jing R X and Qiu X J 2014 Sound absorption of a finite micro-perforated panel backed by a shunted loudspeaker *J. Acoust. Soc. Am.* **135** 231–8
- [20] Lu Z B, Shrestha M and Lau G-K 2017 Electrically tunable and broader-band sound absorption by using micro-perforated dielectric elastomer actuator *Appl. Phys. Lett.* **110** 182901
- [21] Chiu Y H, Cheng L and Huang L 2006 Drum-like silencers using magnetic forces in a pressurized cavity *J. Sound Vib.* **297** 895–915
- [22] Chen X, Xu X C, Ai S G, Chen H S, Pei Y M and Zhou X M 2014 Active acoustic metamaterials with tunable effective mass density by gradient magnetic fields *Appl. Phys. Lett.* **105** 071903
- [23] Zhao J J, Li X H, Wang Y Y, Wang W J, Zhang B and Gai X L 2017 Membrane acoustic metamaterial absorbers with magnetic negative stiffness *J. Acoust. Soc. Am.* **141** 840–6
- [24] Hemmatian M and Sedaghati R 2017 Effect of applied magnetic field on sound transmission loss of MR-based sandwich panels *Smart Mater. Struct.* **26** 025006
- [25] Nguyen H, Zhu R, Chen J K, Tracy S L and Huang G L 2018 Analytical coupled modeling of a magneto-based acoustic metamaterial harvester *Smart Mater. Struct.* **27** 055010
- [26] Hu W Q, Lum G Z, Mastrangeli M and Sitti M 2018 Small-scale soft-bodied robot with multimodal locomotion *Nature* **554** 81–5
- [27] Marin T, Montoya P, Arnache O, Pinal R and Calderon J 2018 Development of magnetite nanoparticles/gelatin composite films for triggering drug release by an external magnetic field *Mater. Des.* **152** 78–87
- [28] Gao W, Wang L L, Wang X Z and Liu H Z 2016 Magnetic driving flowerlike soft platform: biomimetic fabrication and external regulation *ACS Appl. Mater. Interfaces* **8** 14182–9
- [29] Li Y C, Li J C, Li W H and Du H P 2014 A state-of-the-art review on magnetorheological elastomer devices *Smart Mater. Struct.* **23** 123001
- [30] Schmidt A M 2006 Electromagnetic activation of shape memory polymer networks containing magnetic nanoparticles *Macromol. Rapid Commun.* **27** 1168–72
- [31] Belyaeva I A, Kramarenko E Y, Stepanov G V, Sorokin V V, Stadler D and Shamonin M 2016 Transient magnetorheological response of magnetoactive elastomers to step and pyramid excitations *Soft Matter* **12** 2901–13
- [32] Zhu P F, Yang W Y, Wang R, Gao S, Li B and Li Q 2018 4D printing of complex structures with a fast response time to magnetic stimulus *ACS Appl. Mater. Interfaces* **10** 36435–42
- [33] Lum G Z, Ye Z, Dong X G, Marvi H, Erin O, Hu W Q and Sitti M 2016 Shape-programmable magnetic soft matter *Proc. Natl Acad. Sci. USA* **113** E6007–15
- [34] Tang S-Y et al 2018 Versatile microfluidic platforms enabled by novel magnetorheological elastomer microactuators *Adv. Funct. Mater.* **28** 1705484
- [35] Mishra S R, Dickey M D, Velev O D and Tracy J B 2016 Selective and directional actuation of elastomer films using chained magnetic nanoparticles *Nanoscale* **8** 1309–13
- [36] Feng J B, Xuan S H, Lv Z Q, Pei L, Zhang Q C and Gong X L 2018 Magnetic-field-induced deformation analysis of magnetoactive elastomer film by means of DIC, LDV, and FEM *Ind. Eng. Chem. Res.* **57** 3246–54
- [37] Schmauch M M, Mishra S R, Evans B A, Velev O D and Tracy J B 2017 Chained iron microparticles for directionally controlled actuation of soft robots *ACS Appl. Mater. Interfaces* **9** 11895–901
- [38] Mahendran M, Feuchtwanger J, Techapiesanchaenroj R, Bono D and O’Handley R C 2011 Acoustic energy absorption in Ni-Mn-Ga/polymer composites *J. Magn. Mater.* **323** 1098–100
- [39] Hasheminejad S M and Shabanimotlagh M 2010 Magnetic-field-dependent sound transmission properties of magnetorheological elastomer-based adaptive panels *Smart Mater. Struct.* **19** 035006
- [40] Zielinski T G and Rak M 2010 Acoustic absorption of foams coated with MR fluid under the influence of magnetic field *J. Intell. Mat. Syst. Struct.* **21** 125–31
- [41] Rodriguez-Lopez J, Elvira S L, de Espinosa and Freijo F M 2012 Ultrasonic velocity and amplitude characterization of magnetorheological fluids under magnetic fields *J. Magn. Mater.* **324** 222–30
- [42] Hemmatian M and Sedaghati R 2017 Sound transmission analysis of MR fluid based-circular sandwich panels: experimental and finite element analysis *J. Sound Vib.* **408** 43–59
- [43] Boyer T H 1988 The force on a magnetic dipole *Am. J. Phys.* **56** 688–92
- [44] Maa D Y 1998 Potential of microperforated panel absorber *J. Acoust. Soc. Am.* **104** 2861–6